

Original Article

Core-based lipid nanoparticles as a nanoplatform for delivery of near-infrared fluorescent imaging agents

Nadia Anikeeva¹, Yuri Sykulev¹, Edward J Delikatny², Anatoliy V Popov²

¹Department of Microbiology and Immunology and Kimmel Cancer Center, Thomas Jefferson University, Philadelphia, Pennsylvania, USA; ²Department of Radiology, Perelman School of Medicine, University of Pennsylvania, Philadelphia, Pennsylvania, USA

Received June 23, 2014; Accepted August 6, 2014; Epub September 6, 2014; Published September 15, 2014

Abstract: Pyropheophorbide *a* (Pyro) is a near-infrared (NIR) fluorescent dye and photosensitizer with high quantum yield that makes the dye suitable for tumor treatment both as an imaging and therapy agent. We have designed and synthesized a series of a Pyro-based NIR probes, based on the conjugation of Pyro with lipids. The nature of our probes requires the use of a lipophilic carrier to deliver the probes to cancer cell membranes. To address this, we have utilized lipid-based nanoparticles (LNPs) consisting of PEGylated lipids, which form the nanoparticle shell, and a lipid core. To endow the LNPs with targeting properties, nitrilotriacetic acid (NTA) lipids were included in the composition that enables the non-covalent attachment of His-tag targeting proteins preserving their functional activity. We found that the nature of the core molecules influence the nanoparticle size, shelf-life and stability at physiological temperature. Two different Pyro-lipid conjugates were loaded either into the core or shell of the LNPs. The conjugates revealed differential ability to be accumulated in the cell membrane of the target cells with time. Thus, the modular organization of the core-shell LNPs allows facile adjustment of their composition with goal to fine tuning the nanoparticle properties for *in vivo* application.

Keywords: Lipid-based nanoparticles, near-infrared fluorescent probes, lipid-based fluorescent imaging agent, pyropheophorbide *a*

Introduction

Near-infrared (NIR) dyes are advantageous for bioimaging because the fluorescence of NIR chromophores allows for high tissue penetration (millimeters to centimeters deep) and does not overlap with tissue autofluorescence [1, 2]. NIR fluorescence does not involve ionizing radiation, requires only relatively low-cost detection systems, and can be utilized not only for imaging but also for photodynamic therapy (PDT). We have recently developed a series of NIR fluorescent imaging probes based on the NIR dye pyropheophorbide *a* (Pyro) [3-5]. Pyro possesses both NIR fluorescent [3-5] and photoreactive [6, 7] properties. The probes were constructed by conjugation of the Pyro moiety with a phospholipid backbone [3]. One of them, Pyro-phosphatidylethanolamine (Pyro-PtdEtn) is shown in **Figure 1**. This phospholipid conjugate and other hydrophobic conjugates of Pyro, such as Pyro-cholesterol oleate (Pyro-CE-OA)

[8] (**Figure 2**), cannot be solubilized in aqueous solution. Therefore, the application of these NIR probes as well as many other NIR dyes are hampered by their hydrophobicity, and methods of probe delivery have to be developed. The most advantageous way to deliver a hydrophobic probe to a disease site *in vivo* is to utilize a lipid-based nanoparticle platform. Compared to other nanocarriers, lipid-based nanoparticles are distinguished by their self-assembled structure and are biodegradable. Several lipid-based nanocarrier formulations are already approved for clinical applications [9-12].

One approach to develop a lipid-based nanoplatform for the delivery of lipophilic NIR probes is to use lipoproteins, naturally occurring nanoparticles that are present in the human body and play an essential role in transport and control of lipid metabolism. Low-density lipoprotein (LDL) is the most commonly used nanolipoprotein. LDL consists of a phospholipid monolayer,

Core-based lipid nanoparticles

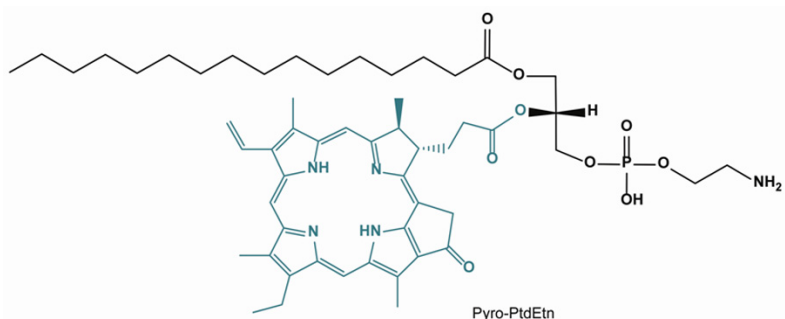


Figure 1. 1-palmitoyl-2-pyropheophorbide-*sn*-glycero-3-phosphatidylethanolamine (Pyro-PtdEtn).

shell containing apolipoproteins and a hydrophobic lipid core containing cholesterol esters and triglycerides. These natural nanoparticles are stable in the blood circulation and have a size (<30 nm) appropriate for avoiding the reticuloendothelial system. Such lipoprotein nano-platforms have been used as a delivery vehicle for a number of lipophilic drugs and imaging agents [13-15]. A major problem to this approach is the existence of receptors recognizing apolipoproteins in different human tissues leading to high background binding. To overcome this drawback, we developed core-based lipid nanoparticles (LNPs) with the structure mimicking the core-shell organization of natural lipoproteins. Metal-ion-chelating lipids were included into the shell for conjugation with targeting proteins. We varied the LNP core composition, NIR lipid probe structure, and the nature of the targeting moiety in order to investigate the LNP properties as a universal multimodal lipid-based nanocarrier for delivery of hydrophobic NIR dyes.

Materials and methods

Reagents

DSPE-PEG (1,2-distearoyl-*sn*-glycero-3-phosphoethanolamine-N-[methoxy (polyethylene glycol)-750], ammonium salt), DOGS-NTA (1,2-dioleoyl-*sn*-glycero-3-((N(5-amino-1-carboxypentyl)iminodiacetic acid) succinyl), ammonium salt) and *N*-BOC Lyso PtdEtn (*N*-Boc16:0 Lyso PE) were purchased from Avanti Polar Lipids, Inc., Alabaster, AL, USA. Cholesterol oleate (CE-OA) was purchased from Sigma Aldrich. Fluo-3 was purchased from Life Technologies, Grand Island, NY USA. *Spirulina pacifica* algae (the starting material for Pyro) was purchased from

Cyanotech Corporation, Kailua-Kona, HI, USA. 5-Androst-17 β -amino-3 β -ol was purchased from Steraloid Inc., Newport, RI. Silica Gel Standard Grade (230x450 mesh) was purchased from Sorbent Technologies, Atlanta, GA, USA. Solvents were purchased from Fisher Scientific; dry solvents were purchased from ACROS Organics. Other reagents/reactants were purchased from

Sigma-Aldrich and used without further purification. Pyropheophorbide-a acid (Pyro) and 5-Androst-17 β -Boc-amino-3 β -yl Oleate (BOC-CE-OA) were synthesized according to [8]. 1-palmitoyl-2-pyropheophorbide-*sn*-glycero-3-phosphoethanolamine (Pyro-PtdEtn) was prepared as previously described [3].

Spectral methods

¹H NMR spectra were recorded using Bruker DMX 360 MHz and DRX 500 MHz spectrometers. MALDI-TOF mass-spectra were recorded with an Applied Biosystems Voyager DE Mass Spectrometer using a positive mode ionization and CHCA (α -cyano-4-hydroxycinnamic acid) or HABA (2-(4-hydroxyphenylazo)benzoic acid) matrix.

Cells

The Epstein-Barr virus (EBV)-transformed B-cell line JY (HLA-A2, B7, Cw7) was grown in RPMI-1640 medium containing 10% fetal calf serum, 10 mM HEPES, 2 mM L-glutamine, 100 U/ml penicillin, 100 μ g/ml streptomycin and 50 μ M β -mercaptoethanol (R10). The human Flu-specific CTL clone CER43 that recognizes the matrix protein peptide GILGFVFTL (GL9) in association with HLA-A2 MHC class I protein [16], was kindly provided by A. Lanzavecchia and was maintained in culture, as previously described [17, 18].

Synthesis

We developed a new two-step synthesis of 5-androst-17 β -pyropheophorbide-amino-3 β -yl oleate (Pyro-CE-OA) (Figure 2). This synthetic pathway is described in the Results section.

Core-based lipid nanoparticles

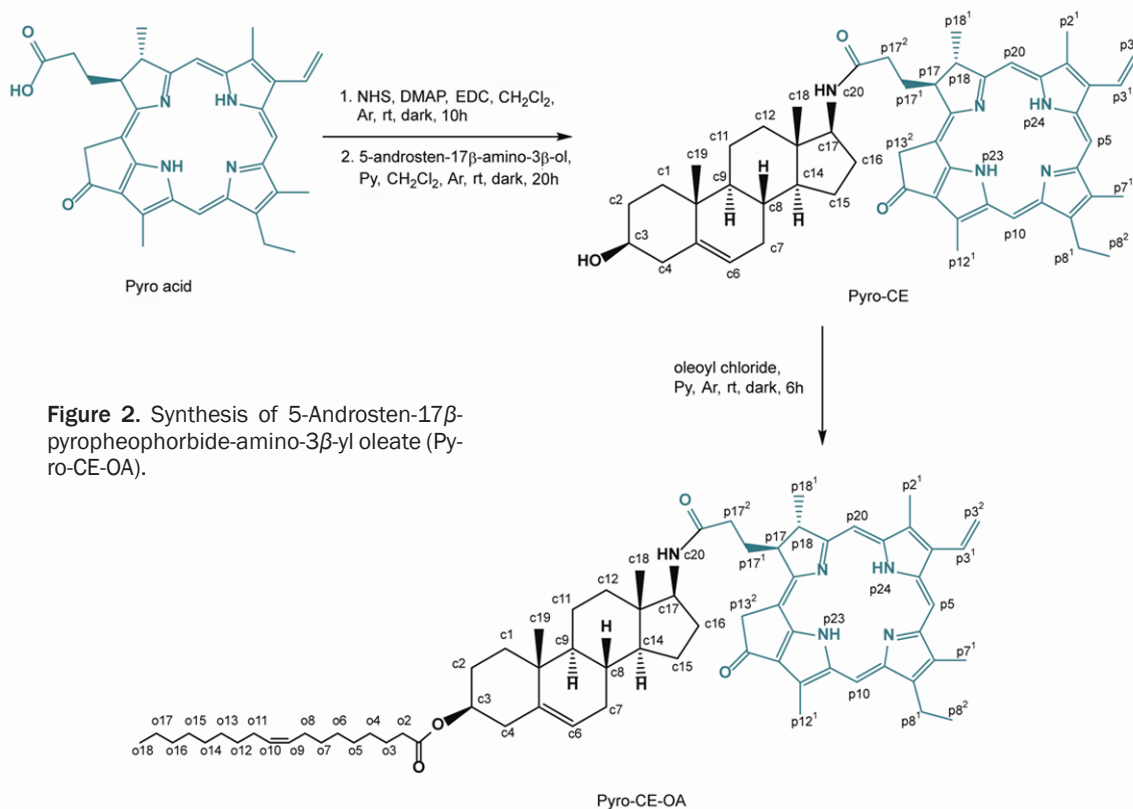


Figure 2. Synthesis of 5-Androsten-17β-pyropheophorbide-amino-3β-yl oleate (Pyro-CE-OA).

5-Androsten-17β-Pyropheophorbide-amino-3β-ol (Pyro-CE)

The synthesis scheme is presented in **Figure 2**. Pyropheophorbide *a* acid (Pyro, 103.0 mg, 0.193 mmol), *N*-hydroxysuccinimide (22.3 mg, 0.193 mmol), EDC (36.9 mg, 0.193 mmol), DMAP (5.8 mg, 0.048 mmol) and dry DCM (50 mL) were placed into a 100 mL round bottom flask (RBF) equipped with a magnetic stirring bar. The reaction mixture was stirred for 10 h in the dark under argon at room temperature. The reaction was monitored by thin layer chromatography (TLC; EtOAc/CHCl₃ 1/1, v/v) until total Pyro conversion into Pyro-SU ester was observed. Then 5-androsten-17β-amino-3β-ol (50 mg, 0.193 mmol) and 2 mL pyridine were added into the flask. The reaction mixture was agitated for more 20 h in dark under argon at room temperature. The volatiles were evaporated and the dark green product was isolated by column chromatography (DCM/EtOAc/MeOH 1/1/0-0.1, v/v/v) in 96% yield (149.3 mg). TLC: one spot, *R*_f=0.15 EtOAc/CHCl₃ 1/5, v/v. ¹H MNR (500 MHz, DMSO-*d*₆, δ): 10.19 (bs, 1H, CE (c) c3-βOH), 9.57, 9.38 and 8.76 (each s, 1H, pyro (p) p5-*H*, p10-*H*, p20-*H*), 8.08 (dd, *J*=11.6

Hz, *J*=17.8 Hz, 1H, p3¹-CH=CH₂), 7.33 (d, *J*=8.6 Hz, 1H, c6-*H*), 6.31 (d, *J*=17.8 Hz, 1H, *trans*-p3²-CH=CHH), 6.18 (d, *J*=11.6 Hz, 1H, *cis*-p3²-CH=CHH), 5.18 (s, 1H, c20-βNH), 5.13 (AB, *A*=5.23, *B*=5.03, *J*_{AB}=19.7 Hz, 2H, p13²-CH₂), 4.59 (q, *J*=7.3 Hz, 1H, p18-*H*), 4.28 (dm, *J*=8.6 Hz, 1H, p17-*H*), 3.71 (q, *J*=7.4 Hz, 2H, p8¹-CH₂), 3.66 (m, 1H, c3-αH), 3.60, 3.42, 3.19, (each s, 3H, p2¹-CH₃, p7¹-CH₃, p12¹-CH₃), 3.24 (m, 1H, c17-αH), 2.67-2.33 (overlap with the solvent signal, m, 4H, p17¹-CH₂ and c4-CH₂), 2.23-1.93 (m, 4H, p17²-CH₂ and c7-CH₂), 1.84-0.78 (multiplets, 15H, c1-CH₂, c2-CH₂, c10-CH, c11-CH₂, c12-CH₂, c13-CH, c14-CH, c15-CH₂, c16-CH₂) 1.81 (d, *J*=7.3 Hz, 3H, p18-CH₃), 1.63 (t, *J*=7.4 Hz, 3H, p8²-CH₃), 0.85 (s, 3H, c19-CH₃), 0.46 (s, 3H, c18-CH₃), -1.75 (s, 2H, p21-NH and p23-NH). MALDI-TOF, *m/z*: (M+Na)⁺ 828.55, calculated for C₅₂H₆₃N₅NaO₃ 828.48 (see [Supporting Information, SI](#)).

5-Androsten-17β-pyropheophorbide-amino-3β-yl oleate (Pyro-CE-OA)

Pyro-CE (120 mg, 0.149 mmol) was dissolved in dry pyridine 50 mL (100 mL RBF), and oleoyl chloride (250 mg, 0.831 mmol) was added. The reaction mixture was agitated for 6 h at room

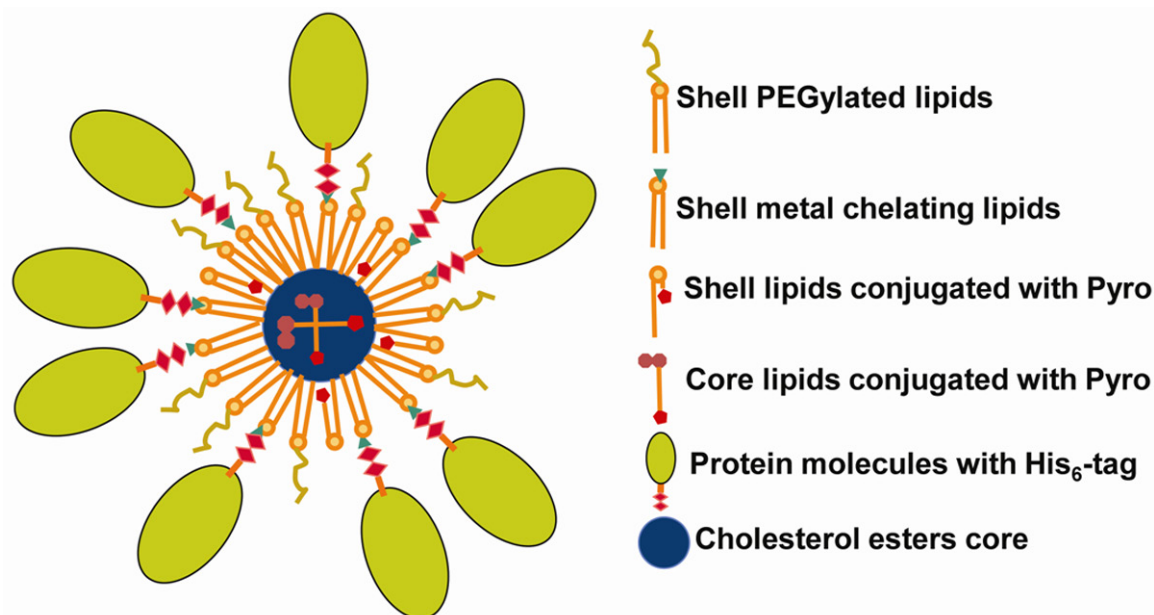


Figure 3. Schematic structure of LNP. PEGylated lipids regulate the solubility of LNPs in water solutions. Metal chelating groups are used for binding protein via a His₆ tag. The His₆ tag controls the protein ligand binding site orientation allowing the attachment of protein molecules without any chemical modification. The Pyro molecules are conjugated to cholesterol or to glycerol based lipids. Fluorescent properties of the molecule will allow *in vivo* molecular imaging and photodynamic therapy. The lipid core composition has influence on the stability of the LNPs.

temperature in the dark under argon gas. The volatiles were evaporated; the remainder was dissolved in chloroform and washed with 0.1 N HCl, followed by 2 times with DI water. The solution was dried over anhydrous Na₂SO₄. The product was isolated by column chromatography (hexanes/EtOAc 1->0/0->1 v/v, V_{hexanes}⁺ V_{EtOAc}⁻=1) in 82.3% yield (131.3 mg). TLC: one spot, R_f=0.4, EtOAc/CHCl₃ 1/5, v/v.

¹H NMR (360 MHz, CDCl₃/CD₃OD, δ): 9.18, 9.06, and 8.41 (each s, 1H, pyro (p), p5-H, p10-H, and p20-H); 7.78 (dd, J=17.8 Hz, J=11.6 Hz, 1H, p3¹-CH=CH₂); 7.14 (d, J=8.6 Hz, 1H, CE (c) c6-H), 6.12 (d, J=17.8 Hz, 1H, *trans*-p3²-CH=CHH); 6.02 (d, J=11.6 Hz, 1H, *cis*-p3²-CH=CHH); 5.20 (m, 2H, oleate (o) o9-H and o10-H, CH=CH), 5.06 (AB, A=5.14, B=4.99, J_{AB}=19.9 Hz, 2H, p13²-CH₂); 4.36 (qd, J=7.3 Hz, J=1.7 Hz 1H, p18-H) 4.17 (m, 2H, p17-H and c3-αH); 3.74 (m, 1H, c17-αH, overlapped with the solvent signal), 3.47, 3.26 and 3.99 (each s, 3H, p2¹-CH₃, p7¹-CH₃ and p12¹-CH₃), 3.63 (q, J=7.7 Hz, 2H, p8¹-CH₂CH₃), 2.65-2.10 (m, 12H, p17¹-CH₂, p17²-CH₂, o8-CH₂, o11-CH₂, c4-CH₂ and c7-CH₂), 2.09-0.83 (m, 39H, o2-CH₂, o3-CH₂, o4-CH₂, o5-CH₂, o6-CH₂, o7-CH₂, o12-

CH₂, o13-CH₂, o14-CH₂, o15-CH₂, o16-CH₂, o17-CH₂, c1-CH₂, c2-CH₂, c11-CH₂, c12-CH₂, c15-CH₂, c16-CH₂, c8-CH, c9-CH, c14-CH), 1.72 (d, J=7.3 Hz, 3H, p18¹-CH₃CH); 1.52 (t, J=7.7 Hz, 3H, p8²-CH₃CH₂), 0.80 (m, 6H, c19-CH₃ and o18-CH₃), 0.35 (s, 3H, c18-CH₃). MALDI-TOF, m/z: (M+Na)⁺ 1093.05, calculated for C₇₀H₉₅N₅NaO₄ 1092.73 (see S1).

Protein expression and purification

Soluble HLA-A2 protein was expressed in S2 cells and "empty" HLA-A2 protein molecules were purified from the culture supernatant as previously described [19, 20]. Soluble HLA-A2 molecules (3-5 mg/ml) were loaded with the peptide of interest overnight at 23-25°C at saturating peptide concentration (10⁻⁴-10⁻⁵ M). HIV RT-derived peptide ILKEPVGHV (IV9) was a generous gift from Herman Eisen (Massachusetts Institute of Technology). GILGFVFTL (GL9) peptide from the matrix protein of influenza virus was synthesized by Research Genetics (Huntsville, AL). The GL9-HLA-A2 complex specifically interacts with the T cell receptor on the surface of the CER-43 CD8 T cell clone, while the IV9-HLA-A2 does not [19, 20]. cDNA coding

Core-based lipid nanoparticles

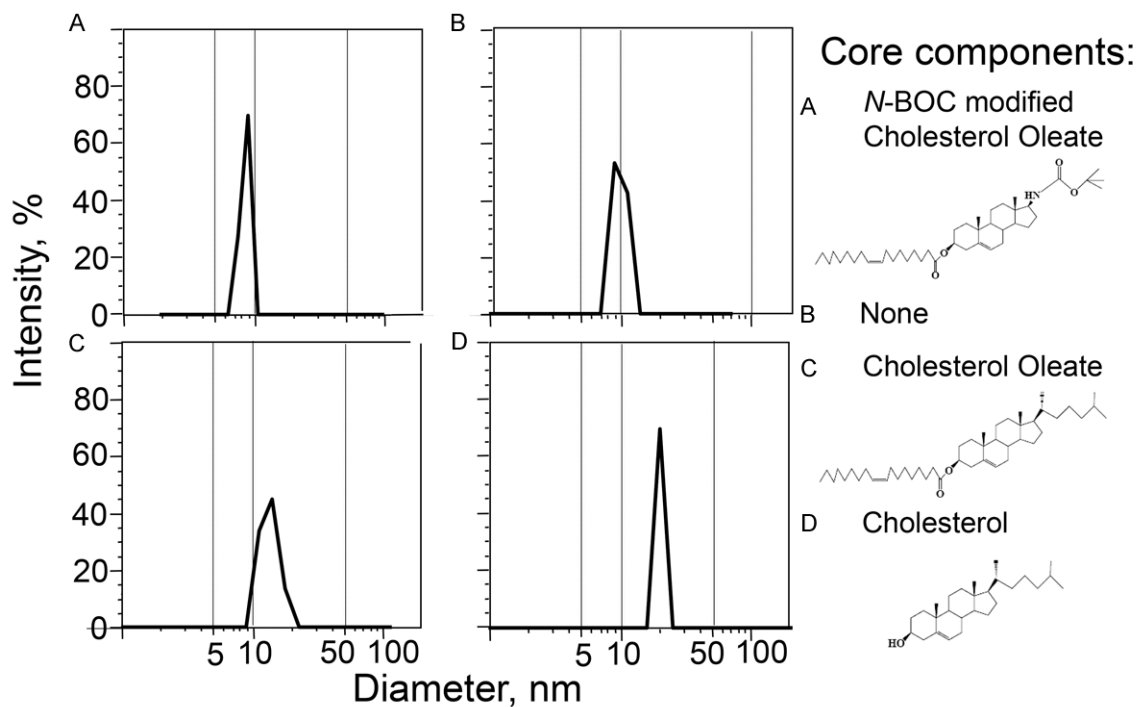


Figure 4. Size distribution of the LNPs (A) with Boc modified cholesterol oleate (BOC-CE-OA) core, (B) without core, (C) with cholesterol oleate core, and (D) with cholesterol core as measured by dynamic light scattering. The structure of corresponding LNP core components are shown on the right side of the Figure.

human ICAM-1 protein was cloned from JY cells. Soluble recombinant human ICAM-1 protein containing a His₆-tag on the C-end of the molecule was produced in the *Drosophila* cell system and purified by affinity chromatography using monoclonal antibody against human ICAM-1 (HB9580, ATCC) as previously described [19, 20]. Protein labeling with Cy5 fluorescent dye was performed according to manufacturer's instructions (Amersham, GE Healthcare). After the labeling procedure the protein was subjected to affinity chromatography on Ni-NTA Agarose (QIAGEN).

LNP preparation

The core components (CE-OA or BOC-CE-OA or cholesterol), DSPE-PEG and DOGS-NTA in dried chloroform were mixed at a molar ratio of 12:68:20. In some cases, fluorescent lipids were added as indicated. Chloroform was removed with an argon stream and the lipid film was additionally dried under vacuum for 3 hours. Lipids were hydrated under argon with intermittent vortexing in hot (65-80°C) HEPES buffered saline (10 mM HEPES, 140 mM NaCl) at a total lipid concentration of 5 mM. The mix-

ture was cooled down in a water bath to room temperature. The suspension was filtered through 0.2 μm mini filters (Sterlitech) and kept under argon at 4°C. To load the NTA moiety with nickel ions, NiSO₄ solution was added to the LNPs at a final concentration of 100 mM. After 30 min of incubation, unbound Ni²⁺ ions were removed by gel filtration on a Bio-Rad mini column loaded with HBS buffer.

To make fluorescently labeled lipid nanoparticles we used either Pyro-CE-OA or Pyro-PtdEtn lipids. Before the assembly of the nanoparticles each fluorescent conjugate was dissolved in chloroform, and the absorption of the solution was measured at 410 nm. Using the extinction coefficient for Pyro ($\epsilon=110,000 \text{ M}^{-1}\text{cm}^{-1}$), [3] we were able to calculate the concentration of the Pyro-lipid conjugate solutions. To avoid self-quenching of the probes, we included only 3% mol of fluorescent molecules into the LNP composition [4].

Light scattering

The size distributions of the LNPs were measured by light-scattering photon correlation spe-

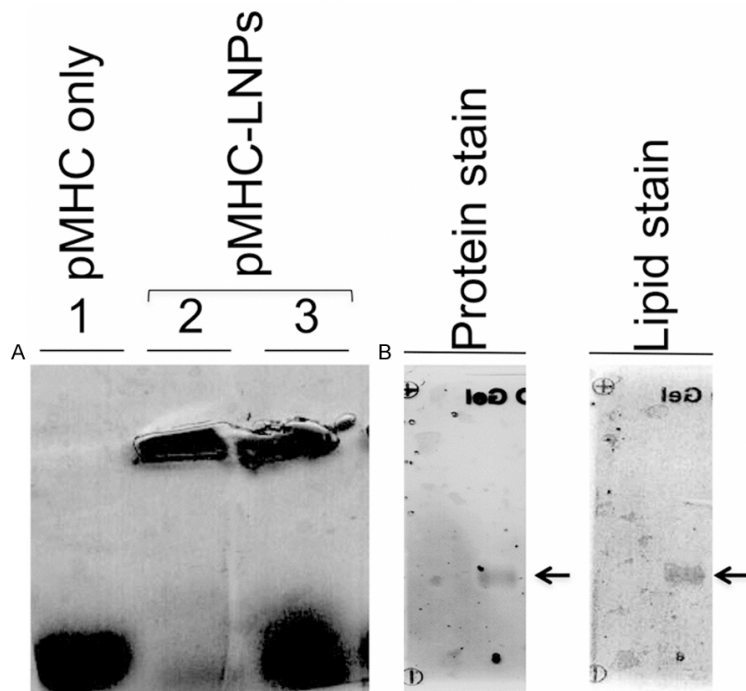


Figure 5. Agarose gel electrophoresis of LNPs. (A) LNPs with cholesterol oleate core were conjugated with Alexa647 labelled pMHC at ratio 5:1 and 1:1 (v/v) as described in the Materials and Methods: unconjugated pMHC-Alexa647 (first line), pMHC-Alexa647 conjugated with LNPs at ratio 1:5 (v/v) (second line), and pMHC-Alexa647 conjugated with LNPs at ratio 1:1 (v/v) (third line). (B) LNPs with cholesterol oleate core were conjugated with unlabeled pMHC and were subjected to electrophoresis using the Paragon electrophoresis kit. The gel was consequently stained with Paragon lipid stain and with Coomassie blue.

ctroscopy (Zetasizer 3000HS, Malvern Instruments, Malvern, UK) utilizing a 10-mW He-Ne laser operating at 633 nm and a detector angle of 90°. The data were modeled assuming spherical particles undergoing Brownian motion [21].

Conjugation of Ni-NTA-LNPs with protein ligands

Conjugate formation was driven by self-assembly between His₆-terminated proteins and LNPs functionalized with Ni-NTA-DOGS lipids as has been described elsewhere [22, 23]. Ni-NTA-LNPs were mixed with protein ligand solution. The mixture was incubated at room temperature for 10 min and diluted with DPBS containing 1% BSA to required ligand concentration.

Agarose gel electrophoresis

LNPs and Cy5 labelled HLA-A2 protein (3 mg/ml) were mixed at ratios 5:1 and 1:1 (v/v) and

incubated at room temperature for 30 min. The samples were mixed with 3% glycerol TBE loading buffer (10 mM Tris-borate with 2 mM EDTA, pH 8.5) immediately prior to use. Unconjugated labeled protein was used as a control. A 15 V/cm electric field was applied to a 1% agarose gel for 20 min. The protein bands were detected by light absorption.

The lipid component of the ICAM-1-LNP conjugate was determined by electrophoresis performed on 0.5% agarose gel (Beckman, Paragon Lipo Kit). The conjugated ICAM-1-LNP samples (1:5 v/v) were subject to electrophoresis in barbital buffer from the kit. After electrophoresis, the gels were fixed in a solution of ethanol-acetic acid-water 60:10:30 (v/v/v) and then stained (5 min) with a 0.15% Coomassie Blue R250 solution. Gels were destained in a solution of methanol-acetic acid-water 35:25:40 (v/v/v) until the Coomassie Blue stains disappeared from the gel

bands. The lipid bands were visualized by staining with Sudan Black B as recommended by the Paragon electrophoresis kit manufacturer. Electrophoretic mobility of the protein bands was compared with electrophoretic mobility of bands stained with the lipid dye.

Flow cytometry analysis

Binding of LNPs/protein conjugates to the surface of live cells was evaluated by flow cytometry as previously described [22, 23]. 2×10^5 CER-43 cells were washed with FACS buffer (DPBS/1% BSA with or without Ca²⁺ and Mg²⁺ as indicated) and suspended in the buffer containing different concentration of protein ligand conjugated with fluorescent LNPs. Control cells were loaded with unconjugated LNPs. In some experiments fluorescent LNPs containing the NTA lipid moiety without Ni²⁺ were utilized as an additional control. The staining procedure was performed at 4°C or 37°C for the indicated time interval. The cells were washed with the

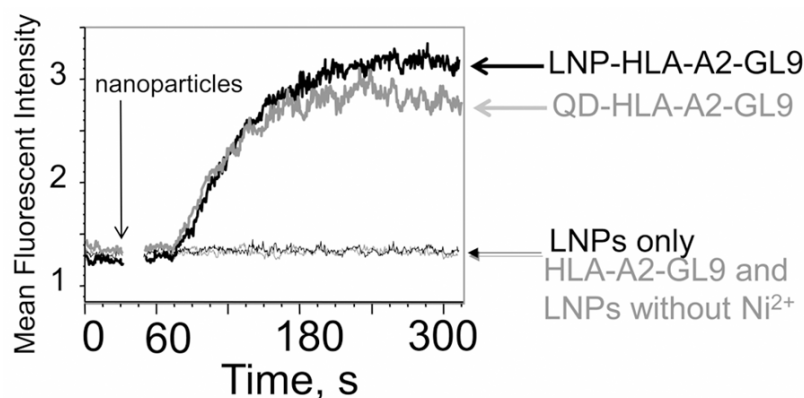


Figure 6. Time-dependent changes in intracellular calcium concentration in CD8⁺ CER43 T cells induced by GL9-HLA-A2 ligands assembled on either LNPs (bold black) or lipid encapsulated QDs (bold grey) scaffolds. Unloaded LNPs (thin black) and cognate pMHC complex mixed with LNPs containing NTA lipid moiety without Ni²⁺ (thin grey) were utilized as negative controls. The concentration of the pHLA-A2 in the extracellular medium was 100 nM. The mean fluorescent intensity of the cells over time was measured by flow cytometry.

buffer, and the samples were analyzed on an Epics XL-MCL flow cytometer (Beckman Coulter, Fullerton, CA) with fluorescence excitation at 633 nm and emission at 675 nm.

Ca²⁺ flux measurements

Measurements of Ca²⁺ flux elicited by specific binding of LNP/pMHC conjugates to CTL surface was performed as described elsewhere [22, 23]. Briefly, CER-43 cells (10⁷ cells/ml) were loaded with Fluo-3 Ca²⁺ sensitive fluorophore as previously described. The cells were washed free of unreacted dye and resuspended in assay buffer (DPBS containing 1 mM CaCl₂, 0.1 mM MgCl₂, 5 mM glucose and 0.025% BSA) at 10⁶ cells/ml. Freshly prepared LNPs conjugated with pMHC were promptly added to 1 ml of the cell suspension. The samples were analyzed on a Coulter Epics XL-MCL flow cytometer. The data collection was initiated as soon as possible following the background measurements. The data were analyzed with FlowJo software. Unloaded LNPs and cognate pMHC complex mixed with LNPs containing NTA lipid moiety without Ni²⁺ were utilized as negative controls.

Microscopy

LNPs loaded with Pyro-PtdEtn fluorophore were used for microscopy analysis. CER-43 cells were stained with fluorescent LNP/pMHC con-

jugates for 3 hr at 37°C. After the washing procedure the cells were resuspended in 100 µl DPBS/1% BSA with Ca²⁺ and Mg²⁺ and placed in 96-well plates with slide glass bottom. The cell fluorescence was analyzed using a wide-field epifluorescence Zeiss Axiovert 200 M inverted microscope with a Roper CoolSnap HQ CCD monochrome camera. The cell samples were excited by the Xenon Lamp at 620/60 nm and the 700/75 nm band pass filter was utilized for emission.

Results

Synthesis of Pyro-CE-OA

We have developed a novel two-step synthesis of 5-Androsten-17β-pyrophephorbide-amino-3β-yl oleate (Pyro-CE-OA). This synthetic pathway is presented in **Figure 2**. A previously described preparation [8] included 1) Boc-protection of the amino group of CE, 2) O-acylation with oleoyl chloride, 3) TFA-mediated Boc-deprotection; 4) conversion of the obtained CE-OA trifluoroacetic salt into a free amine with NaHCO₃ and 5) Pyro-acid activation with 1-hydroxybenzotriazole followed by a coupling with the CE-OA. The final product was isolated by preparative TLC. That procedure afforded several milligrams of the target product with the overall yield 10%. Our new procedure included 1) a one-pot synthesis of Pyro-SU ester (Pyro, NHS, DMAP) followed by a coupling with amino group of CE (5-androsten-17β-amino-3β-ol) and 2) O-acylation with oleoyl chloride. The intermediate and final products were isolated with preparative column chromatography with the overall yield 79% (relative to CE). This new approach affords hundreds of milligrams of Pyro-CE-OA.

Design and assembly of LNPs

The PEG-phosphatidylethanolamine (PEG-PtdEtn) conjugate was chosen as a major constituent of the LNP shell (**Figure 3**). It has been shown that a phospholipid/PEG-PtdEtn mixture

Core-based lipid nanoparticles

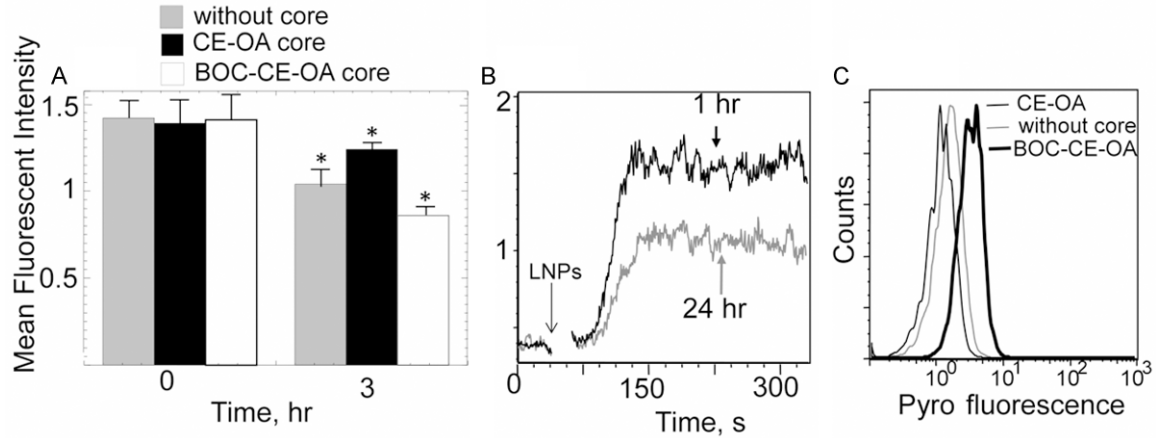


Figure 7. (A) Relative amplitudes of calcium influx induced in CD8⁺ CER43 T cells by Pyro-LNPs-GL9-HLA-A2 conjugates with different cores. The LNPs were pre-incubated at 37 °C in DPBS/1% BSA for the indicated time. Mean±SD are calculated at plateau of the curves (200-250 s), (*)=p<0.01. (B) Time-dependent changes in intracellular calcium concentration in CD8⁺ CER43 T cells induced by Pyro-LNPs-GL9-HLA-A2 conjugate with cholesterol oleate core after preincubation of the LNPs for indicated time at 37 °C. The concentration of the pHLA-A2 in extracellular medium was 100 nM. The mean fluorescent intensity of the cells over time was measured by flow cytometry. (C) Binding of the Pyro-LNPs-GL9-HLA-A2 conjugates with different core to the surface of CER43 T cells. The LNPs conjugates were pre-incubated at 37 °C for 3 hours in DPBS/1% BSA. The concentration of the pHLA-A2 in extracellular medium was 2 μM. The mean fluorescent intensities of the stained cells were measured by flow cytometry.

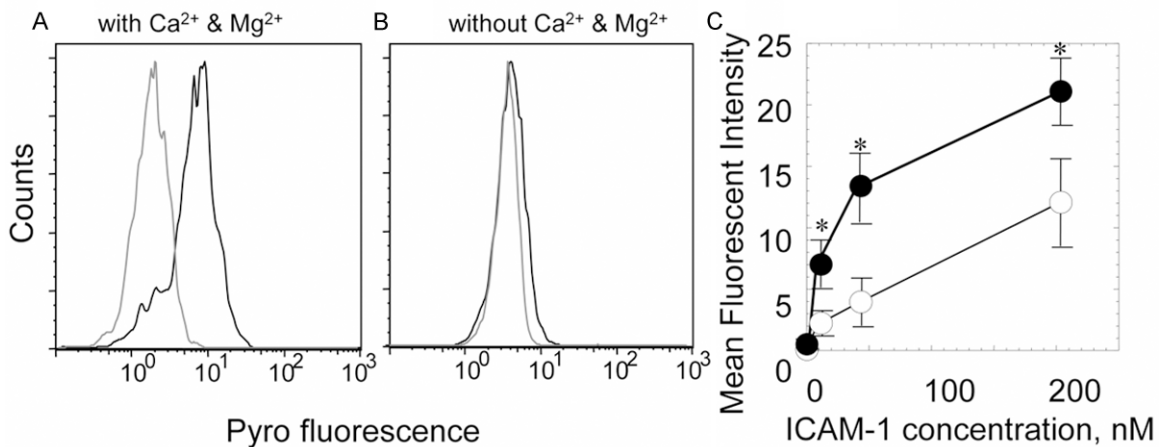


Figure 8. Binding of ICAM-1-LNP-Pyro-PtdEtn to CD8⁺ CER43 T cells expressing cell surface $\alpha_L\beta_2$ integrins that recognize ICAM-1. The cells were incubated with the LNPs conjugate in the presence (A) or absence (B) of Ca²⁺ and Mg²⁺ in the staining buffer. Cells incubated with plain LNPs, i.e., untargeted nanoparticles (grey) were used as negative control. The mean fluorescent intensity of the cells was measured by flow cytometry. Fluorescence was excited at 633 nm and emission collected at 675 nm. (C) The dependence of ICAM-1-NP-Pyro-PtdEtn binding to CER-43 cells on ICAM-1 concentration is shown. Cells incubated with untargeted nanoparticles were utilized as a negative control. Mean±SD is shown, (*)=p<0.05.

forms stable micelles when the PEG-PtdEtn content exceeds a critical limit [24-26]. For the particular mixture of PEG-PtdEtn and NTA-DOGS lipid that was utilized in the present research, the molar content of PEG-PtdEtn lipid should be greater than 60% mol [23, 27], so 67-77% mol of PEG-PtdEtn lipids were used in

the LNP formulation. Small variations in the PEG-PtdEtn molar content depend on the quantity of all other components employed in the LNP composition.

Micelles prepared from PEG-PtdEtn lipids can be loaded with various hydrophobic inorganic

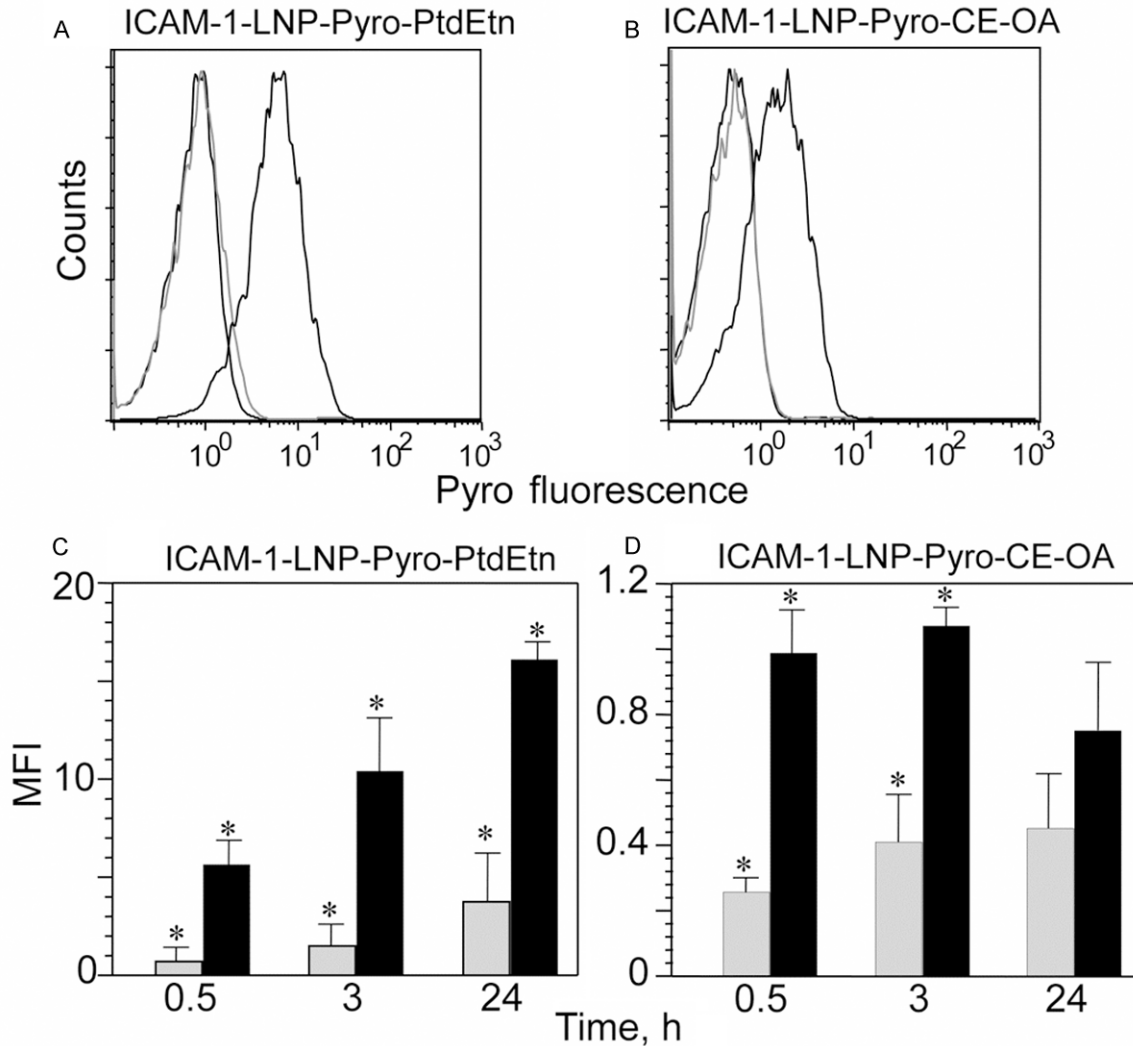


Figure 9. Binding of (A) ICAM-1-LNP-Pyro-PtdEtn and (B) ICAM-1-LNP-Pyro-CE-OA to CD8⁺ CER43 T cells. Binding of the LNPs loaded with irrelevant pHLA-DRB1 protein is shown with grey line. Cells incubated with plain LNPs, i.e., untargeted nanoparticles (grey) were used as negative control. (C and D) Time course of ICAM-1-LNPs (black) binding to CD8⁺ CER43 T cells. CER-43 cells were incubated in the presence of (C) ICAM-1-LNP-Pyro-PtdEtn or (D) ICAM-1-LNP-Pyro-CE-OA for 30 min to 24 h. Cells incubated with untargeted LNPs (grey) were used as negative control. After exhaustive washing, the cells were analyzed by flow cytometry. Mean \pm SD is shown, (*)= $p < 0.05$. The mean fluorescent intensity of the cells was measured by flow cytometry. Fluorescence was excited at 633 nm with emission at 675 nm.

compounds of defined size such as quantum dots (QDs), a semiconductor nanocrystal [28-31]. The inorganic core significantly increases stability of the particles. Natural high-density lipoproteins have sizes similar to PEG-PtdEtn micelles and contain a hydrophobic lipid core consisting mostly of various cholesterol esters and triglycerides. To study how the nature of the core influences LNP stability and size, we designed and assembled LNPs with different core lipids: (i) cholesterol (CE); (ii) cholesterol oleate (CE-OA); (iii) *N*-BOC-protected amino cho-

lesterol oleate (BOC-CE-OA). Based on the structure of high-density lipoprotein, we estimate that core lipids should be around 10-15% mol of total lipid to completely fill the interior LNP space [32, 33]. When the content of the core lipids was increased, lipid precipitation was observed indicating that the nanoparticle core can accommodate a limited amount of cholesterol ester molecules.

To enhance NIR probe delivery to a particular cell type, LNPs should be modified with target-

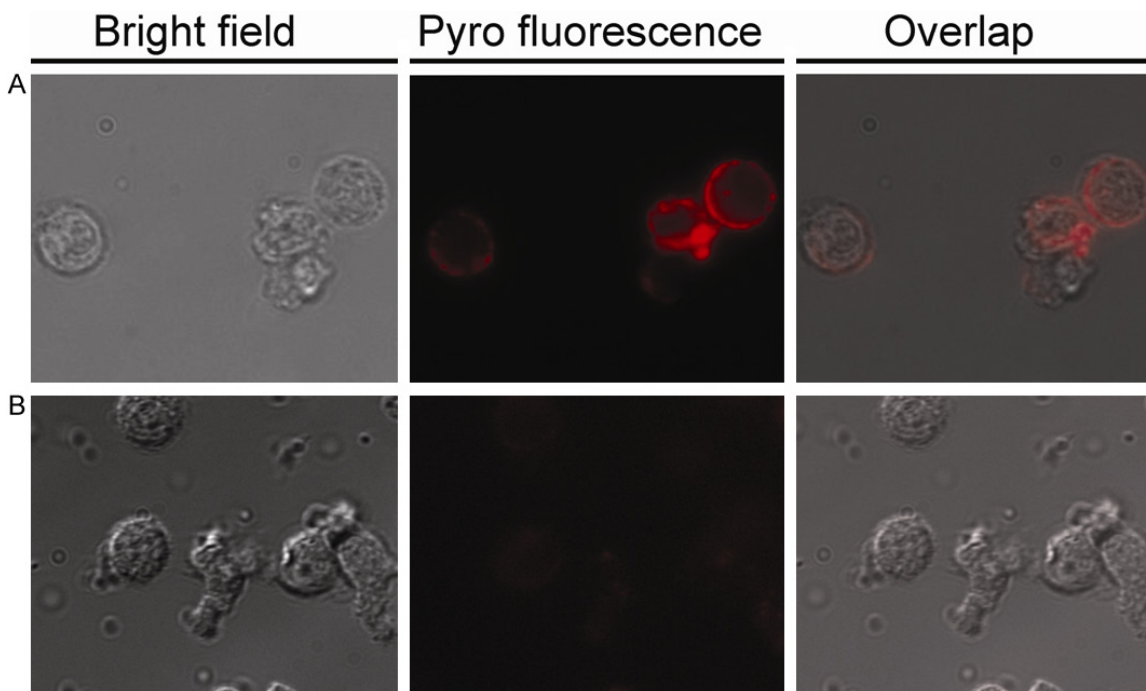


Figure 10. Fluorescent microscopy of CER-43 cells stained with (A) ICAM-1-LNP-Pyro-PtdEtn and (B) plain LNPs. CER-43 cells were stained with LNPs for 3 hr at 37 °C. After washing the samples were used for microscopy on a wide field fluorescence microscope. The near-infrared fluorescence of the probes was excited by Xenon Lamp at 620/60 nm and emission was collected with 700/75 nm band pass filter.

ing ligands. To functionalize the LNPs, metal-chelating lipids (Ni-NTA-DOGS) were included in the particle composition. The Ni-NTA moiety allows conjugation with protein molecules containing polyhistidine-tags. To maximize the density of metal chelating groups, 20% of DOGS-NTA containing lipids were used in the LNP formulation. This density of Ni-NTA moieties increases the strength of interaction between His₆-tagged protein molecules and Ni-NTA groups [34]. Previously we successfully utilized a similar approach for functionalizing PEG-PtdEtn micelle with inorganic core [23, 27].

The lipid-conjugated fluorochromes were introduced into either the core or shell lipids of the LNPs. All fluorescent probes were based on the neutral fluorophore Pyro as a fluorescent probe and photosensitizer with high ¹O₂ quantum yield [35]. Pyro has a far red excitation at 670 nm with near infrared emission at 720 nm that permits increased penetration into tissues. This allows the utilization of the probes *in vivo* for imaging [4] and the potential for killing unwanted cells by photodynamic therapy (PDT). The two various lipid based NIR fluorescent probes were synthesized: (i) Pyro-CE-OA (**Figure**

2) and (ii) Pyro-PtdEtn (**Figure 1**). Pyro-CE-OA contains a cholesterol oleate moiety designed to be incorporated into the LNP core. The Pyro-PtdEtn probe was constructed by conjugation of Pyro to the PtdEtn backbone at the *sn*-2 position of the glycerol backbone in order to be included in LNP shell.

Dependence of LNP size on core composition

The chosen core molecules are distinct from each other by hydrophobicity, conformational flexibility and the ability to form hydrogen bonds. The cholesterol molecules are the most rigid structures. The cholesterol molecules are able to intercalate between the lipids of the outer shell as well as to accumulate into central lipid droplets [36]. CE molecules are the most hydrophobic and possess a high level of conformational flexibility. It has been shown that CE is located in the central core of HDL [36]. BOC-CE-OA molecules have a structure similar to CE but they are endowed with the capability to form intermolecular hydrogen bonds.

The size of the LNPs with different core components was determined by dynamic light scatter-

ing (**Figure 4**). All LNPs had the same shell composition but differ by core content. Fluorescent probes were excluded from the LNPs for these studies because the laser excitation wavelength overlaps with the excitation wavelengths of the fluorescent lipid probes. As is evident from **Figure 4**, the size of the LNPs depends on core composition. The particles with cholesterol core had the largest size (up to 20 nm) presumably due to the intercalation of the cholesterol molecule between the DSPE-PEG outer shell lipids [37]. When cholesterol oleate was used as a core constituent, the LNP size was decreased. LNPs containing cholesterol ester derivatives, BOC-CE-OA, had the smallest size with a narrow distribution pattern.

LNPs core composition also influenced the particle shelf life. While the LNPs without core and LNPs with CE-OA core do not decay for at least 4 weeks storage at 4°C, LNPs with BOC-CE-OA core are completely disassembled during this time with visible sign of lipid precipitation.

Attachment of protein ligands

The LNP platform permits the conjugation of multiple ligands with the particles. The formation of multivalent nanoparticle conjugates allows the potential achievement of optimal performance for therapeutic and imaging applications and is especially important when weak ligand-receptor interactions are involved [27, 38]. Herein, we employed two protein ligands, Intercellular Adhesion Molecule 1 (ICAM-1) and human leukocyte antigen A0201 (HLA-A2) associated with antigenic peptide, which have low intrinsic affinity to their corresponding cell surface receptors, $\alpha_L\beta_2$ integrin and T cell receptor (TCR). Both receptors form high density clusters on the leucocyte surface enhancing selectivity of nanoparticle targeting [39-42].

His₆ tags were placed on the C-end of the ligand molecules to secure uniform positioning of the protein relative to the nanoparticle surface and guarantee productive interaction with corresponding receptors on a cell surface. We previously successfully conjugated ICAM-1 and HLA-A2 soluble molecules with lipid encapsulated quantum dots, and utilized the conjugates for specific staining of human T cell clones [23, 43].

The conjugate formation was driven by metal-affinity interaction between His₆ tag of protein

ligands and the Ni-NTA-moiety of the lipid shell. The ligand attachment to the LNPs was monitored by agarose gel electrophoresis. The Cy5 labeled proteins were mixed with the CE-OA-LNPs at different ratios with the aim of achieving ligand saturation, and the mixtures were subjected to agarose gel electrophoresis. The amount of protein needed to saturate the LNPs was determined by agarose gel electrophoresis. The protein bands were visualized by dye adsorption (**Figure 5A**). It has previously been shown that the electrophoretic mobility of heavily PEGylated nanoparticles are small or negligible due to the thickness of the polymer coating and the consequent shielding of nanoparticle surface charge. Consistent with this, the LNPs conjugated with the ligands showed insignificant electrophoretic mobility compared with free protein. The insulation of the lipid head charge with PEG prevents movement of the conjugated LNPs while the negatively charged protein migrated toward the cathode. Saturation of the LNPs with protein was achieved when 15 µg protein were mixed with 1 µl of LNPs suspension at 5 mM lipid concentration. After further increasing of the ligand amount in the mixture, the strong band of the free protein was observed (**Figure 5A**, third line).

Conjugate formation was confirmed by utilizing the Lipo Electrophoresis kit (Beckman Coulter) that enables the visualization of the lipid component of the LNPs by the Paragon lipid stain. As is evident from **Figure 5B** lipid and protein staining were overlapped.

It is important to confirm that conjugated ligands are active after association with LNPs. To demonstrate this, HLA-A2 protein was chosen as a targeting ligand. After loading with GL9 peptide, the pMHC ligand was specifically recognized by T cell receptor on the surface of CER-43 T cells. It has been shown that soluble pMHC monomer is not stimulatory, and induction of TCR-mediated signaling requires TCR engagement by at least a bivalent pMHC ligand [44, 45]. Conjugation of the pMHC with nanoparticles results in the formation of multivalent pMHC ligands, whose recognition induces an increase in intracellular Ca²⁺ concentration in T cells. This approach was successfully exploited in our previous work to monitor binding specificity and functionality of lipid encapsulated QD nanoparticles conjugated with GL9-HLA-A2 [23, 43]. As is evident from **Figure 6**,

the CE-OA-LNP-GL9-HLA-A2 conjugate induces an increase in intracellular calcium in T cells to a similar extent as the GL9-HLA-A2-QDs conjugate. In control experiments, the LNPs were not loaded with Ni^{2+} and consequently were incapable to form conjugates with His₆-tagged proteins. The mixture of the unloaded LNPs and cognate GL9-HLA-A2 did not induce Ca^{2+} influx in the T cells (**Figure 6**). These results demonstrate that LNPs can be easily conjugated with His₆-containing proteins using incorporated Ni-NTA-DOGS lipids, and that the proteins retain their functional activity after association with LNPs.

Effect of the core on LNP shelf-life and stability at physiological temperature

Changing core lipid composition can affect the hydrophobic interaction in the LNPs interior altering the stability of the nanoparticles. To assay stability, the LNP-GL9-HLA-A2 conjugates were incubated in DPBS, for 3 hr at 37°C. We used LNPs containing CE-OA and BOC-CE-OA molecules, which differ in structure only by the polar Boc moiety. Stability was compared by the functional calcium assay (**Figure 7A** and **7B**) or by measuring the binding ability of the conjugates (**Figure 7C**). Whereas the LNPs with the CE-OA core do not significantly change the magnitude of the Ca^{2+} flux in CER-43 cells after 3 hours at 37°C, cells treated with LNPs with the BOC-CE-OA core demonstrated a decrease in the magnitude of the Ca^{2+} flux (**Figure 7A**). Moreover, LNPs with the CE-OA core effectively induced the CTL response even after 24-hour incubation at 37°C (**Figure 7B**). Assessment of the LNP-GL9-HLA-A2 conjugates binding confirms our initial results. These data indicates that LNPs with CE-OA core have improved stability in agreement with the shelf life measurements of unconjugated LNPs. Thus, for all further experiments LNPs with a CE-OA core were utilized.

Interaction of the targeted Pyro-LNPs with specific cells in vitro

To endow the targeted particles with NIR fluorescent properties two different Pyro conjugates were used: (i) core targeted Pyro-CE-OA conjugate and (ii) shell targeted Pyro-PtdEtn conjugate. Pyro can form aggregates at high concentration, so based on our previous experience the amount of fluorescent lipid in the

nanoparticle composition did not exceed 3% mol %.

The LNPs were functionalized with ICAM-1 adhesion molecules that recognized $\alpha_L\beta_2$ integrin receptor (LFA-1). CER-43 human T cells overexpress LFA-1 on their cell surface. The LFA-1 molecule contains a single divalent cation binding site, called the I domain [46]. Interaction of LFA-1 with ICAM-1 ligand depends on the presence of Mg^{2+} and Ca^{2+} . As is evident from **Figure 8A**, ICAM-1 loaded nanoparticles specifically interacted with the surface of CER43 cells in the presence of 1 mM Mg^{2+} and Ca^{2+} in the staining buffer. Removing the divalent cations from the buffer led to a decrease in this interaction (**Figure 8B**). This demonstrates the specificity of ICAM-1-LNPs binding to the cell surface. Although the intrinsic affinity of the interaction between ICAM-1 molecules and their receptor is low [47], the staining was highly sensitive ($K_{\text{avidity}} \sim 8$ nM) presumably due to the multivalent nature of ICAM-1-LNPs (**Figure 8C**).

The amplitude of the fluorescence depends on the nature of Pyro-lipid conjugates. The cells incubated with ICAM-1-LNP-Pyro-PtdEtn had a higher mean fluorescence intensity (MFI) relative to background (**Figure 9A**) than ICAM-1-LNP-Pyro-CE-OA treated cells (**Figure 9B**). To understand better the difference in the LNPs containing different fluorescent conjugates we investigated changes of the cell MFI as function of time (**Figure 9**). As is evident from **Figure 9C**, the fluorescence of the cells incubated with ICAM-1-LNP-Pyro-PtdEtn dramatically increased while fluorescence of the cells incubated with ICAM-1-LNPs-Pyro-CE-OA stayed constant (**Figure 9D**). This suggests that shell-associated fluorescent lipids can exchange with cell membrane lipids allowing accumulation of Pyro-PtdEtn conjugates in the cell membrane of target cells, thus increasing intensity of cell staining [48]. Pyro-CE-OA conjugate lipids on the other hand, have a low ability to accumulate in the cell membrane. Furthermore, after releasing the contents of endocytosed LNPs in the cytoplasm, Pyro-CE-OA conjugate lipids could self-quench due to aggregation in aqueous solution [49].

The conclusion is supported by analysis of fluorescence images of CER-43 cells incubated with the ICAM-1-LNP-Pyro-PtdEtn at 37°C (**Figure 10**). Interaction of ICAM-1-LNP-Pyro-

PtdEtn with the surface of CER-43 cells leads to accumulation of the fluorescent dye mostly in the cell membrane (**Figure 10A**). Binding of the untargeted LNPs to the CER-43 cells was not observed thus confirming the specificity of the process (**Figure 10B**). The intensity of the staining the LNPs increased with time (data not shown). Thus, the imaging data confirm that specific targeting of T cell surface with ICAM-1-LNP-Pyro-PtdEtn lead to accumulation of Pyro-PtdEtn conjugates in the cell membrane.

Discussion

We have recently developed a series of porphyrin-based NIR fluorescent probes, which are analogs of cell membrane lipids and have potential to be used as photodynamic therapy (PDT) agents [3, 5]. In previous studies liposome formulations were employed for probe delivery, and the resulting unilamellar vesicles were utilized for imaging of tumors in a mouse model [4]. The phospholipid liposomes have a relatively large size (>70 nm) leading to their preferential accumulation in tumor perivascular space and little permeation into the tumor [50]. This is useful for NIR imaging purposes but less promising for PDT where the malignant cell bulk needs to be targeted.

The main factors preventing formation of stable phospholipid liposomes of sub-70 nm size are membrane rigidity and edge tension [51]. To overcome this obstacle, we decided to utilize micelle structures spontaneously formed by PEGylated phospholipids in aqueous solutions [52]. Overall, the phospholipid PEGylated micelles are less stable in the blood circulation compared with phospholipid PEGylated liposomes [53]. The influence of the phospholipid structure and size of the PEG head on the properties of the micelle are very well known and optimal shell phospholipid structure can be chosen for particular needs [54]. To tune the stability of the nanocarriers in blood circulation, we introduced cholesterol or cholesterol esters into the LNPs core composition. The resulting particles have a micellar structure with significantly smaller size (<20 nm) compared to the liposomes we utilized previously. Surprisingly, the size of the LNPs revealed a strong dependence on core lipids showing a difference of 2.5 fold between the smallest (BOC-CE-OA) and the largest (cholesterol) core. The

behavior of hydrophobic core components of different nature has been previously investigated for spheroidal high density lipoprotein (HDL) [36, 55]. The hydrophobic CE-OA molecules are located in the core of the HDL and have minimal overlap with water, whereas most of the cholesterol is located just below the phospholipids forming the outer layer with a small but significant concentration of cholesterol also found in the core of the HDL [36]. It is suggested that cholesterol molecules are able to intercalate between the alkyl chains of the outer phospholipids shell of LNPs while cholesterol oleate molecules concentrate mostly in the central part of the micelle, thus explaining the difference in the size of CE-OA or cholesterol containing LNPs. Intriguingly, the LNPs with the BOC-CE-OA core, which contains lipids with more a polar moiety than CE-OA, possess the smallest size. Presumably, the formation of the hydrogen bonds between the BOC-CE-OA molecules leads to more unfavorable entropy of the micelle self-assembly process and consequently to destabilization of the particles.

Our results also showed that changes in the core lipids have a strong impact not only on size of the LNPs but also on their shelf-life and stability at physiological temperature. It has been shown that *in vitro* stability of micelles is inversely correlated with residency time of a lipid monomer in a micelle [56]. A highly hydrophobic micelle core provides a large activation barrier to monomer desorption from the micelle leading to great stability of the particles [56-58]. Thus, the greater stability of the CE-OA containing LNPs might be explained by higher hydrophobicity of the CE-OA core forming molecules compared with BOC-CE-OA lipids. The nanoparticle core hydrophobicity and/or the relative rigidity of the nanoparticle core have an important effect on blood residency time but the nature of the effect could be more complex in character than in a cellular free system [54]. Particularly, the size and rigidity of the LNPs should allow them to adapt to the size and shape of the fenestrations in leaky tumor vascularity leading to a significant effect on particle accumulation in the solid tumor.

After reaching the tumor tissue, LNPs should have the ability to specifically deliver PDT agents to cancer cells leaving normal otherwise cells intact. To actively target unwanted cells

and to enhance probe delivery, the LNPs were functionalized with Ni-NTA containing lipids (DOGS-NiNTA), which allows protein ligands containing His₆ tags to be conjugated without applying harsh conjugation chemistry. As expected, after ligation with low affinity ligands (0.01-1 μ M) the resulting multivalent LNPs specifically interacted with the receptors on the cell surface with high avidity. This data is in agreement with the results of several other groups that have utilized NTA containing nanoliposomes for immobilization of His-tagged proteins [23, 43, 59-63].

Both NIR probes utilized in our study were based on Pyropheophorbide-*a* but differed by the nature of the conjugated lipid (phospholipid vs cholesterol oleate). Pyro conjugated with phospholipids shows better kinetics and a higher magnitude of cellular accumulation compared with the cholesterol based probe. While phospholipids are the major constituent of all cell membranes, cholesterol esters are stored and transported largely in bulk lipid phases such as intracellular lipid storage droplets and serum lipoproteins [64]. The difference in kinetics of the probes accumulation could be explained by the intrinsic ability of the Pyro-PtdEtn probe to intercalate into the target cell membranes for producing signal. This localization of Pyro-PtdEtn probe in the cellular membrane is supported by fluorescent microscopy. Pyro-CE-OA conjugates have a higher chance to be delivered in cell cytoplasm. In aqueous solutions Pyro and their conjugates with lipids can form aggregates resulting in fluorescent reabsorption and intermolecular quenching [4, 7]. The singlet oxygen quantum yields of aggregated species are lower than those of monomers, reducing their PDT efficiency. Thus, the Pyro-PtdEtn probe has the ability to be a more potent imaging agent and photosensitizer than Pyro-CE-OA probe.

Conclusions and future perspective

The goal of this study was to develop an appropriate carrier for delivering of a hydrophobic NIR dye, i.e. pyropheophorbide *a* conjugated with a lipid, to the membrane of targeted cells. For this purpose, lipid-based nanoparticles with a core-shell structure were utilized. Changing the core composition allowed us to tune the LNP properties. In particular, the usage of a

cholesterol oleate core improved the stability of the particles at physiological temperature and their shelf-life. The LNPs loaded with shell but not core targeted Pyro-conjugates revealed great ability to accumulate in the cell membrane. These properties increase the potential of the probe for application *in vivo* as an imaging and PDT agent. It is not clear at present what the impact of the *in vivo* environment will be on the LNPs targeting capability. To overcome this obstacle, we have also developed a Pyro-based "smart" probe that possesses targeting properties. The probe was constructed by conjugation of Pyro and a quencher (Black Hole Quencher 3) to a phosphatidylethanolamine backbone [3-5]. The probe is recognized and cleaved by phosphatidylcholine-specific phospholipase C, which shows enhanced accumulation in different types of cancers [65-68]. Enzymatic cleavage dequenches the Pyro fluorescence and restores the Pyro photoreactivity resulting in a pronounced NIR fluorescence signal recovery and photodynamic cytotoxicity. The developed LNPs are well suited to serve as an *in vivo* nanocarrier for this advanced "smart" probe. Furthermore, the lipid based nanoparticles loaded with core will be tested as vehicles for targeted delivery of lipophilic fluorinated potential drugs and imaging agents that we have been developing in recent years [69-75].

Acknowledgements

Financial support was provided by the DoD (W81XWH-08-1-0716 (AVP) and NIH grants R01-CA114347 (EJD), R01-CA129176 (EJD), R01-AI52812 (YS), R21-CA131973 (YS). The authors acknowledge the assistance of Dr. T.V. Lebedeva (TJU, UPenn) for ICAM-1 expression and of Dr. H. Choi (UPenn) for dynamic light scattering analysis.

Disclosure of conflict of interest

None.

Address correspondence to: Dr. Anatoliy V Popov, Department of Radiology, Perelman School of Medicine, University of Pennsylvania, Room 317, Anatomy Chemistry Building, 3620 Hamilton Walk, Philadelphia PA, 19104-4799 USA. Tel: 1-215-746-8761; Fax: 1-215-746-8764; E-mail: avpopov@mail.med.upenn.edu

References

- [1] Nolting DD, Gore JC and Pham W. Near-infrared dyes: probe development and applications in optical molecular imaging. *Curr Org Synth* 2011; 8: 521-534.
- [2] Sevick-Muraca EM. Translation of near-infrared fluorescence imaging technologies: emerging clinical applications. *Annu Rev Med* 2012; 63: 217-231.
- [3] Popov AV, Mawn TM, Kim S, Zheng G and Delikatny EJ. Design and Synthesis of Phospholipase C and A2-Activatable Near-Infrared Fluorescent Smart Probes. *Bioconjugate Chem* 2010; 21: 1724-1727.
- [4] Mawn TM, Popov AV, Beardsley NJ, Stefflova K, Milkevitch M, Zheng G and Delikatny EJ. In Vivo Detection of Phospholipase C by Enzyme-Activated Near-Infrared Probes. *Bioconjugate Chem* 2011; 22: 2434-2443.
- [5] Mawn TM, Popov AV and Delikatny EJ. A quantitative continuous enzyme assay of intramolecularly quenched fluorogenic phospholipase substrates for molecular imaging. *Anal Biochem* 2012; 422: 96-102.
- [6] Liu T, Wu LY, Choi JK and Berkman CE. In vitro targeted photodynamic therapy with a pyropheophorbide-a conjugated inhibitor of prostate-specific membrane antigen. *Prostate* 2009; 69: 585-594.
- [7] Sun X and Leung WN. Photodynamic therapy with pyropheophorbide-a methyl ester in human lung carcinoma cell: Efficacy, localization and apoptosis. *Photochem Photobiol* 2002; 75: 644-651.
- [8] Zheng G, Li H, Zhang M, Lund-Katz S, Chance B and Glickson JD. Low-Density Lipoprotein Reconstituted by Pyropheophorbide Cholesteryl Oleate as Target-Specific Photosensitizer. *Bioconjugate Chem* 2002; 13: 392-396.
- [9] Peer D, Karp JM, Hong S, Farokhzad OC, Margalit R and Langer R. Nanocarriers as an emerging platform for cancer therapy. *Nat Nanotechnol* 2007; 2: 751-760.
- [10] Puri A, Loomis K, Smith B, Lee JH, Yavlovich A, Heldman E and Blumenthal R. Lipid-based nanoparticles as pharmaceutical drug carriers: from concepts to clinic. *Crit Rev Ther Drug Carrier Syst* 2009; 26: 523-580.
- [11] Souto EB and Muller RH. Lipid nanoparticles: effect on bioavailability and pharmacokinetic changes. *Handb Exp Pharmacol* 2010; 197: 115-141.
- [12] Zolnik BS, Gonzalez-Fernandez A, Sadrieh N and Dobrovolskaia MA. Nanoparticles and the immune system. *Endocrinology* 2010; 151: 458-465.
- [13] Nikanjam M, Blakely EA, Bjornstad KA, Shu X, Budinger TF and Forte TM. Synthetic nano-low density lipoprotein as targeted drug delivery vehicle for glioblastoma multiforme. *Int J Pharm* 2007; 328: 86-94.
- [14] Glickson JD, Lund-Katz S, Zhou R, Choi H, Chen IW, Li H, Corbin I, Popov AV, Cao W, Song L, Qi C, Marotta D, Nelson DS, Chen J, Chance B and Zheng G. Lipoprotein nanoplatform for targeted delivery of diagnostic and therapeutic agents. *Mol Imaging* 2008; 7: 101-110.
- [15] Glickson JD, Lund-Katz S, Zhou R, Choi H, Chen IW, Li H, Corbin I, Popov AV, Cao W, Song L, Qi C, Marotta D, Nelson DS, Chen J, Chance B and Zheng G. Lipoprotein nanoplatform for targeted delivery of diagnostic and therapeutic agents. *Adv Exp Med Biol* 2009; 645: 227-239.
- [16] Gotch F, Rothbard J, Howland K, Townsend A and McMichael A. Cytotoxic T lymphocytes recognize a fragment of influenza virus matrix protein in association with HLA-A2. *Nature* 1987; 326: 881-882.
- [17] Valitutti S, Mueller S, Dessing M and Lanzavecchia A. Different responses are elicited in cytotoxic T lymphocytes by different levels of T cell receptor occupancy. *J Exp Med* 1996; 183: 1917-1921.
- [18] Lebedeva T, Anikeeva N, Kalams SA, Walker BD, Gaidarov I, Keen JH and Sykulev Y. Major histocompatibility complex class I-intercellular adhesion molecule-1 association on the surface of target cells: Implications for antigen presentation to cytotoxic T lymphocytes. *Immunology* 2004; 113: 460-471.
- [19] Anikeeva N, Lebedeva T, Krogsgaard M, Tetin SY, Martinez-Hackert E, Kalams SA, Davis MM and Sykulev Y. Distinct Molecular Mechanisms Account for the Specificity of Two Different T-Cell Receptors. *Biochemistry* 2003; 42: 4709-4716.
- [20] Anikeeva N, Lebedeva T, Sumaroka M, Kalams SA and Sykulev Y. Soluble HIV-specific T cell receptor: expression, purification and analysis of the specificity. *J Immunol Methods* 2003; 277: 75-86.
- [21] Goldberg WI. Dynamic light scattering. *Am J Phys* 1999; 67: 1152-1160.
- [22] Anikeeva N, Somersalo K, Sims TN, Thomas VK, Dustin ML and Sykulev Y. Distinct role of lymphocyte function-associated antigen-1 in mediating effective cytolytic activity by cytotoxic T lymphocytes. *Proc Natl Acad Sci U S A* 2005; 102: 6437-6442.
- [23] Anikeeva N, Gakamsky D, Schoeller J and Sykulev Y. Evidence that the density of self peptide-MHC ligands regulates T-cell receptor signaling. *PLoS One* 2012; 7: e41466.
- [24] Bedu-Addo FK, Tang P, Xu Y and Huang L. Interaction of polyethylene glycol-phospholipid conjugates with cholesterol-phosphatidylcholine

Core-based lipid nanoparticles

- mixtures: sterically stabilized liposome formulations. *Pharm Res* 1996; 13: 718-724.
- [25] Edwards K, Johnsson M, Karlsson G and Sil-vander M. Effect of polyethyleneglycol-phos-pholipids on aggregate structure in prepara-tions of small unilamellar liposomes. *Biophys J* 1997; 73: 258-266.
- [26] Ashok B, Arleth L, Hjelm RP, Rubinstein I and Oenyueksel H. In vitro characterization of PE-Gylated phospholipid micelles for improved drug solubilization: Effects of PEG chain length and PC incorporation. *J Pharm Sci* 2004; 93: 2476-2487.
- [27] Anikeeva N, Mareeva T, Liu W and Sykulev Y. Can oligomeric T-cell receptor be used as a tool to detect viral peptide epitopes on infected cells? *Clin Immunol* 2009; 130: 98-109.
- [28] Carion O, Mahler B, Pons T and Dubertret B. Synthesis, encapsulation, purification and cou-pling of single quantum dots in phospholipid micelles for their use in cellular and in vivo im-aging. *Nat Protoc* 2007; 2: 2383-2390.
- [29] Dubertret B, Skourides P, Norris DJ, Noireaux V, Brivanlou AH and Libchaber A. In vivo imag-ing of quantum dots encapsulated in phospho-lipid micelles. *Science* 2002; 298: 1759-1762.
- [30] Dabbousi BO, Rodriguez-Viejo J, Mikulec FV, Heine JR, Mattoussi H, Ober R, Jensen KF and Bawendi MG. (CdSe)ZnS Core-Shell Quantum Dots: Synthesis and Optical and Structural Characterization of a Size Series of Highly Lu-minescent Materials. *J Phys Chem B* 1997; 101: 9463-9475.
- [31] Mattoussi H, Mauro JM, Goldman ER, Ander-son GP, Sundar VC, Mikulec FV and Bawendi MG. Self-Assembly of CdSe-ZnS Quantum Dot Bioconjugates Using an Engineered Recombi-nant Protein. *J Am Chem Soc* 2000; 122: 12142-12150.
- [32] Silva RA, Huang R, Morris J, Fang J, Gracheva EO, Ren G, Kontush A, Jerome WG, Rye KA, Da-vidson WS. Structure of apolipoprotein A-I in spherical high density lipoproteins of different sizes. *Proc Natl Acad Sci U S A* 2008; 105: 12176-12181.
- [33] Zhang Z, Chen J, Ding L, Jin H, Lovell JF, Corbin IR, Cao W, Lo PC, Yang M, Tsao MS, Luo Q and Zheng G. HDL-Mimicking Peptide-Lipid Nano-particles with Improved Tumor Targeting. *Small* 2010; 6: 430-437.
- [34] Blanchette CD, Fischer NO, Corzett M, Bench G and Hoeprich PD. Kinetic Analysis of His-Tagged Protein Binding to Nickel-Chelating Nanolipoprotein Particles. *Bioconjugate Chem* 2010; 21: 1321-1330.
- [35] MacDonald IJ, Morgan J, Bellnier DA, Paszkie-wicz GM, Whitaker JE, Litchfield DJ and Dough-erty TJ. Subcellular localization patterns and their relationship to photodynamic activity of pyropheophorbide-a derivatives. *Photochem Photobiol* 1999; 70: 789-797.
- [36] Vuorela T, Catte A, Niemela PS, Hall A, Hyvonen MT, Marrink SJ, Karttunen M and Vattulainen I. Role of lipids in spheroidal high density lipopro-teins. *PLoS Comput Biol* 2010; 6: e1000964.
- [37] Parker A, Miles K, Cheng KH and Huang J. Lat-eral distribution of cholesterol in dioleoylphos-phatidylcholine lipid bilayers: cholesterol-phos-pholipid interactions at high cholesterol limit. *Biophys J* 2004; 86: 1532-1544.
- [38] Shokeen M, Pressly ED, Hagooley A, Zheleznyak A, Ramos N, Fiamengo AL, Welch MJ, Hawker CJ and Anderson CJ. Evaluation of Multivalent, Functional Polymeric Nanoparticles for Imag-ing Applications. *ACS Nano* 2011; 5: 738-747.
- [39] Hong S, Leroueil PR, Majoros IJ, Orr BG, Baker JR and Banaszak Holl MM. The Binding Avidity of a Nanoparticle-Based Multivalent Targeted Drug Delivery Platform. *Chem Biol* 2007; 14: 107-115.
- [40] Wang S and Dormidontova EE. Nanoparticle targeting using multivalent ligands: computer modeling. *Soft Matter* 2011; 7: 4435-4445.
- [41] Zhong L, Zeng G, Lu X, Wang RC, Gong G, Yan L, Huang D and Chen ZW. NSOM/QD-based di-rect visualization of CD3-induced and CD28-enhanced nanospatial coclustering of TCR and coreceptor in nanodomains in T cell activation. *PLoS One* 2009; 4: e5945.
- [42] Bakker GJ, Eich C, Torreno-Pina JA, Diez-Ahedo R, Perez-Samper G, van Zanten TS, Figdor CG, Cambi A and Garcia-Parajo MF. Lateral mobility of individual integrin nanoclusters orches-trates the onset for leukocyte adhesion. *Proc Natl Acad Sci U S A* 2012; 109: 4869-4874, S4869/4861-S4869/4810.
- [43] Beal AM, Anikeeva N, Varma R, Cameron TO, Vasiliver-Shamis G, Norris PJ, Dustin ML and Sykulev Y. Kinetics of early T cell receptor sig-naling regulate the pathway of lytic granule de-livery to the secretory domain. *Immunity* 2009; 31: 632-642.
- [44] Boniface JJ, Rabinowitz JD, Wulfig C, Hampl J, Reich Z, Altman JD, Kantor RM, Beeson C, Mc-Connell HM and Davis MM. Initiation of signal transduction through the T cell receptor re-quires the peptide multivalent engagement of MHC ligands. *Immunity* 1998; 9: 459-466.
- [45] Cebecauer M, Guillaume P, Mark S, Michielin O, Boucheron N, Bezard M, Meyer BH, Segura JM, Vogel H and Luescher IF. CD8+ Cytotoxic T Lymphocyte Activation by Soluble Major Histo-compatibility Complex-Peptide Dimers. *J Biol Chem* 2005; 280: 23820-23828.
- [46] Diamond MS and Springer TA. The dynamic regulation of integrin adhesiveness. *Curr Biol* 1994; 4: 506-517.

Core-based lipid nanoparticles

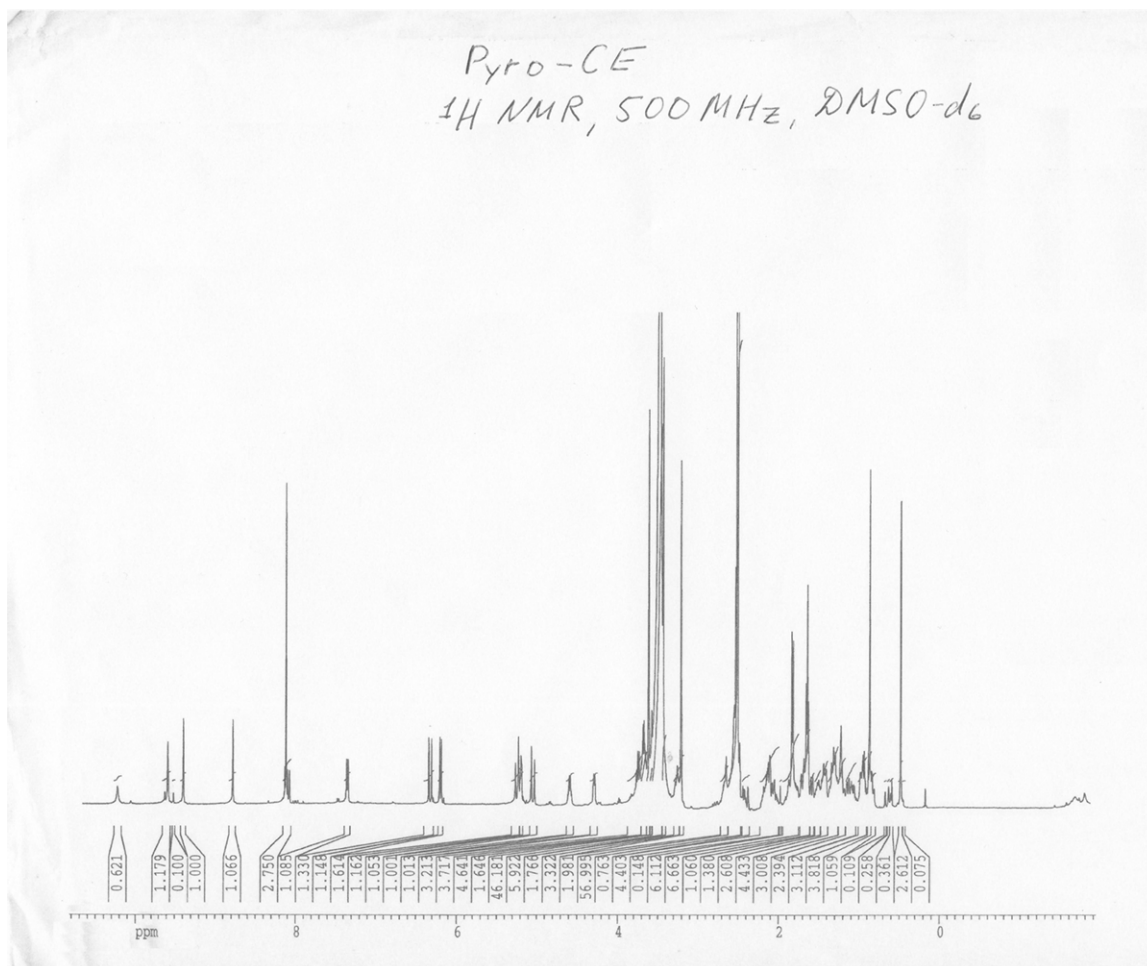
- [47] Sarantos MR, Raychaudhuri S, Lum AFH, Staunton DE and Simon SI. Leukocyte Function-associated Antigen 1-mediated Adhesion Stability Is Dynamically Regulated through Affinity and Valency during Bond Formation with Intercellular Adhesion Molecule-1. *J Biol Chem* 2005; 280: 28290-28298.
- [48] Chen H, Kim S, Li L, Wang S, Park K and Cheng JX. Release of hydrophobic molecules from polymer micelles into cell membranes revealed by Forster resonance energy transfer imaging. *Proc Natl Acad Sci U S A* 2008; 105: 6596-6601.
- [49] Fabiano AS, Allouche D, Sanejouand YH and Paillous N. Synthesis of a new cationic pyropheophorbide derivative and studies of its aggregation process in aqueous solution. *Photochem Photobiol* 1997; 66: 336-345.
- [50] Perrault SD, Walkey C, Jennings T, Fischer HC and Chan WCW. Mediating Tumor Targeting Efficiency of Nanoparticles Through Design. *Nano Lett* 2009; 9: 1909-1915.
- [51] Hernandez-Zapata E, Martinez-Balbuena L and Santamaria-Holek I. Thermodynamics and dynamics of the formation of spherical lipid vesicles. *J Biol Phys* 2009; 35: 297-308.
- [52] Sawant RR and Torchilin VP. Polymeric micelles: polyethylene glycol-phosphatidylethanolamine (PEG-PE)-based micelles as an example. *Methods Mol Biol* 2010; 624: 131-149.
- [53] Torchilin VP. Lipid-core micelles for targeted drug delivery. *Curr Drug Delivery* 2005; 2: 319-327.
- [54] Sun X, Rossin R, Turner JL, Becker ML, Joralemon MJ, Welch MJ and Wooley KL. An assessment of the effects of shell cross-linked nanoparticle size, core composition, and surface pegylation on in vivo biodistribution. *Bio-macromolecules* 2005; 6: 2541-2554.
- [55] Koivuniemi A, Heikela M, Kovanen PT, Vattulainen I and Hyvonen MT. Atomistic simulations of phosphatidylcholines and cholesteryl esters in high-density lipoprotein-sized lipid droplet and trilayer: clues to cholesteryl ester transport and storage. *Biophys J* 2009; 96: 4099-4108.
- [56] Kastantin M, Ananthanarayanan B, Karmali P, Ruoslahti E and Tirrell M. Effect of the Lipid Chain Melting Transition on the Stability of DSPE-PEG(2000) Micelles. *Langmuir* 2009; 25: 7279-7286.
- [57] Brown RE. Spontaneous lipid transfer between organized lipid assemblies. *Biochim Biophys Acta* 1992; 1113: 375-389.
- [58] Wimley WC and Thompson TE. Exchange and flip-flop of dimyristoyl phosphatidylcholine in liquid-crystalline, gel and two-component, two-phase large unilamellar vesicles. *Biochemistry* 1990; 29: 1296-1303.
- [59] Chikh GG, Li WM, Schutze-Redelmeier MP, Meunier JC and Bally MB. Attaching histidine-tagged peptides and proteins to lipid-based carriers through use of metal-ion-chelating lipids. *Biochim Biophys Acta* 2002; 1567: 204-212.
- [60] Huang Z, Park JI, Watson DS, Hwang P and Szoka FC Jr. Facile Synthesis of Multivalent Nitrotriacetic Acid (NTA) and NTA Conjugates for Analytical and Drug Delivery Applications. *Bioconjugate Chem* 2006; 17: 1592-1600.
- [61] Platt V, Huang Z, Cao L, Tiffany M, Riviere K and Szoka FC Jr. Influence of Multivalent Nitrotriacetic Acid Lipid-Ligand Affinity on the Circulation Half-Life in Mice of a Liposome-Attached His6-Protein. *Bioconjugate Chem* 2010; 21: 892-902.
- [62] Ruger R, Muller D, Fahr A and Kontermann RE. In vitro characterization of binding and stability of single-chain Fv Ni-NTA-liposomes. *J Drug Target* 2006; 14: 576-582.
- [63] van Broekhoven CL and Altin JG. The novel chelator lipid 3(nitrotriacetic acid)-ditetradecylamine (NTA3-DTDA) promotes stable binding of His-tagged proteins to liposomal membranes: Potent anti-tumor responses induced by simultaneously targeting antigen, cytokine and costimulatory signals to T cells. *Biochim Biophys Acta* 2005; 1716: 104-116.
- [64] Smaby JM and Brockman HL. Regulation of cholesteryl oleate and triolein miscibility in monolayers and bilayers. *J Biol Chem* 1987; 262: 8206-8212.
- [65] Paris L, Cecchetti S, Spadaro F, Abalsamo L, Lugini L, Pisanu ME, Iorio E, Natali PG, Ramoni C and Podo F. Inhibition of phosphatidylcholine-specific phospholipase C downregulates HER2 overexpression on plasma membrane of breast cancer cells. *Breast Cancer Res* 2010; 12: R27.
- [66] Iorio E, Ricci A, Bagnoli M, Pisanu ME, Castellano G, Di Vito M, Venturini E, Glunde K, Bhujwala ZM, Mezzanzanica D, Canevari S and Podo F. Activation of Phosphatidylcholine Cycle Enzymes in Human Epithelial Ovarian Cancer Cells. *Cancer Res* 2010; 70: 2126-2135.
- [67] Spadaro F, Ramoni C, Mezzanzanica D, Miotti S, Alberti P, Cecchetti S, Iorio E, Dolo V, Canevari S and Podo F. Phosphatidylcholine-Specific Phospholipase C Activation in Epithelial Ovarian Cancer Cells. *Cancer Res* 2008; 68: 6541-6549.
- [68] Abalsamo L, Spadaro F, Bozzuto G, Paris L, Cecchetti S, Lugini L, Iorio E, Molinari A, Ramoni C and Podo F. Inhibition of phosphatidylcholine-

Core-based lipid nanoparticles

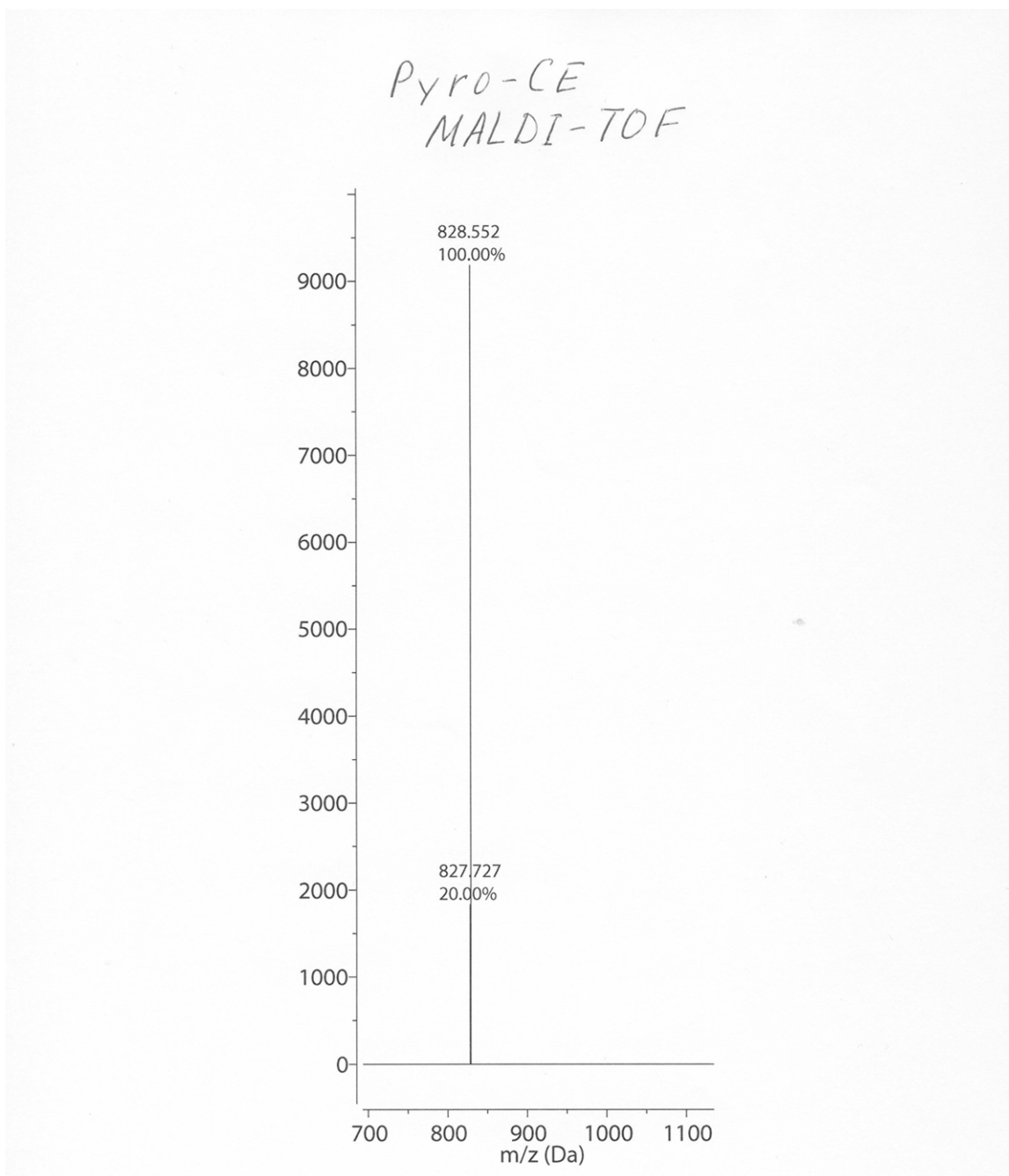
- specific phospholipase C results in loss of mesenchymal traits in metastatic breast cancer cells. *Breast Cancer Res* 2012; 14: R50.
- [69] Luzina EL and Popov AV. Synthesis and anticancer activity of N-bis(trifluoromethyl)alkyl-N'-thiazolyl and N-bis(trifluoromethyl)alkyl-N'-benzothiazolyl ureas. *Eur J Med Chem* 2009; 44: 4944-4953.
- [70] Luzina EL and Popov AV. Anticancer activity of N-bis(trifluoromethyl)alkyl-N'-(polychlorophenyl) and N'-(1,2,4-triazolyl) ureas. *Eur J Med Chem* 2010; 45: 5507-5512.
- [71] Luzina EL and Popov AV. Synthesis, evaluation of anticancer activity and COMPARE analysis of N-bis(trifluoromethyl)alkyl-N'-substituted ureas with pharmacophoric moieties. *Eur J Med Chem* 2012; 53: 364-373.
- [72] Luzina EL and Popov AV. Synthesis of 1-arylsulfonyl-4-bis(trifluoromethyl)alkyl semicarbazides as potential physiologically active compounds. *J Fluorine Chem* 2013; 148: 41-48.
- [73] Kachur AV, Popov AA, Delikatny EJ, Karp JS and Popov AV. Synthesis of ¹⁸F-labeled phenolphthalein and naphtholphthalein. *J Fluorine Chem* 2013; 151: 1-6.
- [74] Kachur AV, Popov AV, Karp JS and Delikatny EJ. Direct Fluorination of Phenolsulfonphthalein: A Method for Synthesis of Positron-Emitting Indicators for In Vivo pH Measurement. *Cell Biochem Biophys* 2013; 66: 1-5.
- [75] Kachur AV, Sardelis D, Bentzley C, Popov AV, Delikatny EJ and Karp J. Synthesis and characterization of fluorinated derivatives of cresolsulfonphthalein. *J Fluorine Chem* 2013; 145: 112-117.

Supporting information

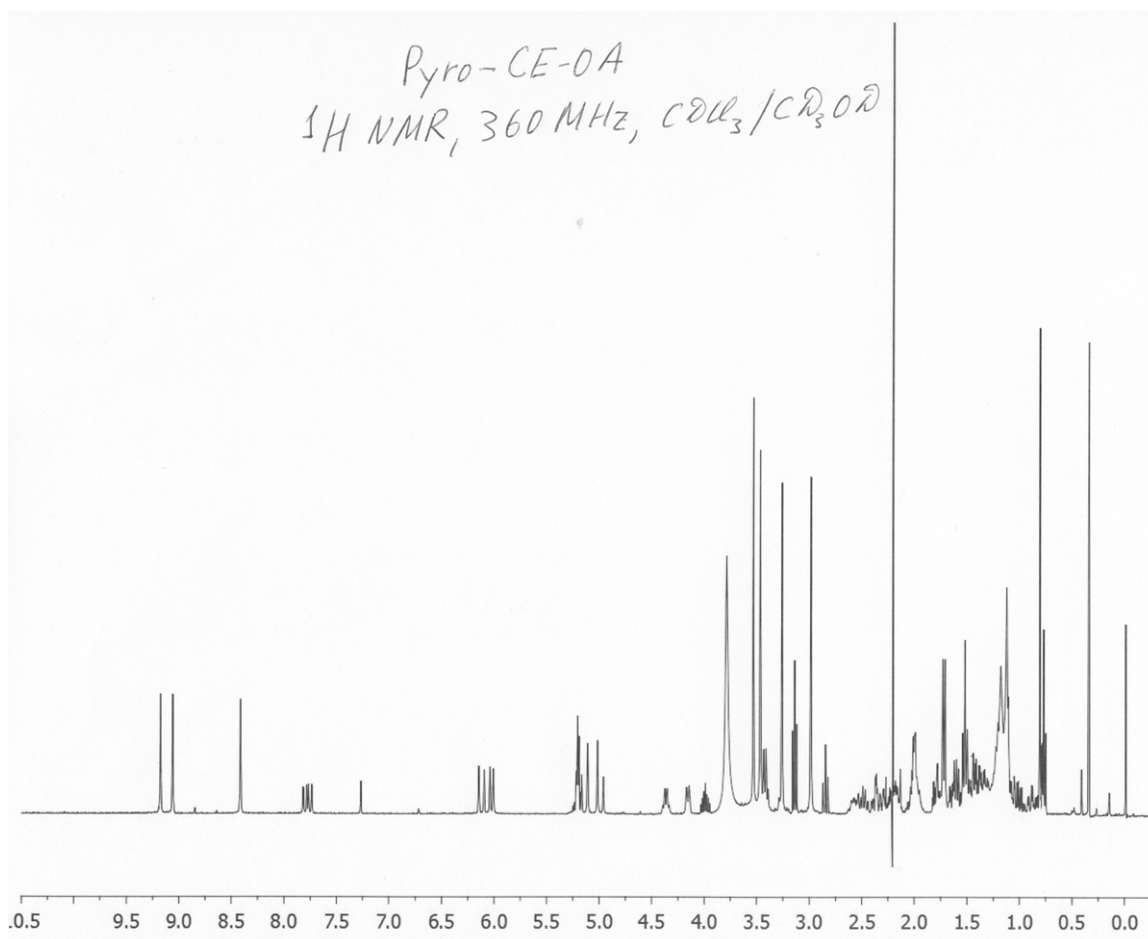
^1H NMR and Mass-spectra



Core-based lipid nanoparticles



Core-based lipid nanoparticles



Core-based lipid nanoparticles

Pyro-CE-OA
MALDI-TOF

